Modulation of magnetization precession trajectories by perpendicular magnetic anisotropy in CoFeB thin films

Angshuman Deka, Iori Tanaka, John Rex Mohan, Yasuhiro Fukuma

Department of Computer Science and Electronics, Kyushu Institute of Technology, 680-4 Kawazu, Iizuka 820-8502, Japan

Precession trajectories during excitation of magnetization dynamics play an important role in determining spinwave propagation, emission power of spin torque oscillator and spin current generated by spin pumping. So far, however, comparatively little information has emerged on the effect of perpendicular magnetic anisotropy (PMA) on dynamical magnetization trajectories. The effect of PMA on magnetization dynamics has become particularly important since the discovery of voltage control of magnetic anisotropy in CoFeB/MgO junctions. This motivates us to investigate the effect of PMA on dynamical magnetization trajectories of CoFeB thin films using micromagnetic simulations. The ellipticity of the trajectories are found to have a strong monotonous dependence on PMA. On the other hand, the area of such elliptical trajectories, which determine the spin current generation, show a non-monotonous change with respect to PMA. This area can be expected to be maximum for the case where ellipticity is ~ 0.5.

***Index Terms*— Magnetodynamics, ferromagnetic resonance, magnetization precession trajectories, magnetic anisotropy, spin pumping, spin waves.**

I. Introduction

Efficient generation of spin current, which is the flow of spin angular momentum of electrons, is a crucial area of research in the field of spintronics because effect of Joule heating due to large charge current density in the nano-dimensions. Generation of spin current has been targeted from various mechanisms such as spin Hall effect [1] or non-local spin injection technique [2]. Additionally, it was demonstrated that temperature gradients in ferromagnets can be used to generate spin currents via spin Seebeck effect [3]. Yet another technique to generate spin current is via spin pumping wherein magnetization dynamics inside a ferromagnet can be used to emit spin current [4]. The advantage of spin pumping is that the excitation of magnetization dynamics can be achieved using electric-fields in ferromagnetic metal-oxide junctions [5-7]. Such a feature of spin pumping promises to make it a low power alternative for efficient spin current generation.

Intrinsic properties like resistivity of Ta has been shown to be dominant in determining the spin to charge interconversion via spin Hall effect [8]. Additionally, interface engineering by MgO insertion between NiFe and Ag layers was shown to greatly improve spin current generation in lateral spin valves [9]. Such studies demonstrate that in addition to the factors such as external field and applied power, internal parameters are just as important in determining efficiency of spin current generation from ferromagnetic nanostructures. As is evident from the mechanism of spin pumping, trajectories during excitation of magnetization dynamics play an important role in determining the amount of spin current generated during the process. In addition to spin pumping, the trajectories also determine the excitation efficiency of spin waves and emission power of spin torque oscillators. Although magnetization trajectories can be controlled to a great extent by the amplitudes of static and oscillating fields [10-12], two major internal factors that limit the dynamical magnetization components are the demagnetizing and magnetic anisotropy fields. Recently it was reported that electric-fields can control the effective demagnetizing fields in metallic ferromagnets via voltage controlled magnetic anisotropy (VCMA) [13]. Using this mechanism, a variety of ultrafast dynamical magnetization phenomena such as ferromagnetic resonance (FMR) excitation [5,6], magnetization switching [14] and spin wave excitation [7] have been demonstrated. Of particular interest is the demonstration of VCMA in CoFeB/MgO junctions which exhibit large interfacial perpendicular magnetic anisotropy (PMA) and tunneling magnetoresistance [15,16].

In this study we investigated the magnetization trajectories during FMR as a function of PMA in CoFeB thin films using Landau-Lifshutz-Gilbert (LLG) micromagnetic simulations. FMR simulations are performed in a frequency sweep mode by keeping the magnetization constant in an in-plane direction as shown in Fig. 1(a). Due to the presence of demagnetizing fields, the trajectories were elliptical. The ellipticity of the trajectories are strongly dependent on the PMA of the ferromagnet. The area of the magnetization trajectories is found to be maximum around the value of PMA for which the ellipticity of the trajectory is ~ 0.5. The corresponding easy direction of magnetization is in the film plane, which is contrary to the expectation that area of trajectory would be maximum for samples where effective demagnetizing fields are zero. The origin of such a behavior is found to be due to a non-monotonous change of x-axial magnetization component with respect to PMA.

III. Ferromagnetic Resonance Simulations

Simulations were performed using LLG micromagnetic simulator on samples of dimensions 100 nm × 100 nm × 1 nm [17]. Damping constant was taken as $\alpha = 0.02$. In order to excite FMR using frequency sweep mode, we applied an rf-magnetic field along the x-direction $h_{rf,x}$ and a static external field $H_{ex,y}$ to pin the magnetization direction along the y-axis. The frequency of the rf-magnetic field was varied from 1 to 20 GHz in steps of 0.2 GHz. The amplitude of $\mu_o h_{rf,x} = 0.1$ mT was used throughout, except the power dependent analysis where $\mu_o h_{rf,x}$ was varied from 0.1 mT to 1.0 mT. The saturation magnetization of the sample was taken as $M_s = 1500$ mT, while the PMA energy $K_{u,2}$ was varied from 0 to 9 $\times 10^5$ Jm^{-3}, in order to match typically reported values for CoFeB/MgO junctions [18]. Using the relation $K_{u2} = \frac{M_s H_p}{2}$, we can estimate that the corresponding PMA fields H_p are varied from 0 to 1500 mT.

III. Results And Discussions

Figure 1(b) shows the resulting real and imaginary parts of the FMR spectra when $K_{u,2} = 0$ and $\mu_o H_{ex,y} = 100$ mT. We can obtain the resonance frequency f_{res} by fitting the data I_{FMR} using:

$$I_{FMR} = \frac{L \times df^2}{(f - f_{res})^2 + df^2} + \frac{D \times df \times (f - f_{res})}{(f - f_{res})^2 + df^2}, \qquad (1)$$

where L and D are the Lorentzian and dispersive parts of the spectra, f_{res} is the resonance frequency and df is the linewidth of the FMR signal. Upon fitting the FMR spectra for the range of $K_{u,2}$ studied, we notice that the f_{res} varies from 11 GHz to 1 GHz as $\mu_o H_p$ is increased from 0 to 1500 mT as shown in Fig. 1(c). From the H_p dependence of f_{res}, we can estimate the out-of-plane demagnetizing field for our sample as $\mu_o H_d = 1400$ mT, using the simple form of Kittel equation: $f_{res} = \gamma\sqrt{(H_d - H_p + H_{ex,y}) H_{ex,y}}$, where $\gamma = 0.0298$ GHz.mT^{-1}. Ideally for thin films where the x- and y- dimensions are infinite compared to the thickness along z-axis, we have demagnetizing components $(\eta_x, \eta_y, \eta_z) = (0,0,1)$. This results in the demagnetizing field to be equal to the saturation magnetization i.e. $H_d = \eta_z M_s = M_s$ [19]. However, in nanostructures where the lateral dimensions are comparable to the thicknesses, we can have $\eta_x \neq 0$ and $\eta_y \neq 0$. Since the components of demagnetizing tensor are related by $\eta_x^2 + \eta_y^2 + \eta_z^2 = 1$, we will have $\eta_z < 1$. This can explain our observation of $\mu_o H_d < 1500$ mT.

Magnetic free energy of a ferromagnetic thin film is given by the sum of Zeeman, demagnetizing and anisotropy energy terms. A frequency dependent FMR study helps us to fix the Zeeman energy of the ferromagnetic system, during our investigation of the effect of PMA on the magnetization trajectories. Figure 2 shows the corresponding three dimensional plots when PMA is varied from $\mu_o H_p = 0$ to $\mu_o H_p = 1500$ mT at $\mu_o H_{ex,y} = 100$ mT. One of the major characteristics that we can observe from Fig. 2(a), where $\mu_o H_p = 0$, is that the trajectory is elliptical as seen from the x-z plane projections in the same figure. This is due to the presence of a strong effective demagnetizing field of magnitude $\mu_o H_{d,eff} = \mu_o H_d = 1400$ mT. Such a field restricts the movement of the magnetization in the out-of-plane direction as a result of which we obtain an elliptical trajectory with $M_z < M_x$.

The presence of PMA enables us to reduce $H_{d,eff}$ in the sample which is given by the difference of H_d and H_p. In CoFeB/MgO junctions, PMA arises due to hybridization between the 3*d* orbitals of Fe and 2*p* orbitals of O atoms at the interface [ref]. Such a PMA in CoFeB/MgO junctions can be large enough to overcome H_d so that $H_{d,eff}$ becomes negative and the easy axis shifts from the in-plane to the out-of-plane direction. Figure 2(b) and 2(c) shows the trajectories when the sample has $\mu_o H_p = 1200$ mT, 1365 mT. We can see that as the $\mu_o H_{d,eff}$ is reduced, the z-component of the magnetization during precession increases compared to Fig. 2(a). The increase in the z-component can be understood in terms of a reduced demagnetizing field which allows the magnetization to preccess more freely around the external magnetic field. When the H_p overcomes the H_d, i.e., when the easy axis of the sample is perpendicular to the film plane, the magnetization motion would be restricted in the in-plane direction. Therefore, we observe that the long axis of the ellipse changes from the in-plane direction to the out-of plane when $\mu_o H_p = 1500$ mT as shown in Fig. 2 (d).

Magnetization components are constrained by the relation $M_x^2 + M_y^2 + M_z^2 = M_s^2$, due to which the tip of the elliptical magnetization trajectory lies on the surface of a sphere, also known as the Bloch's sphere. This results in a time dependent component of magnetization parallel to the external magnetic field M_y whose frequency is twice of the transverse magnetization components M_x and M_z, as shown in Fig. 3(a). It is worth mentioning here that such a component of magnetization that oscillates at twice the resonance frequency can be utilized for non-linear parametric FMR excitation when the $h_{rf,x}$ is similar to the FMR linewidth dH {ref}. Uniform mode FMR corresponds to spinwave vector k = 0 and therefore cannot be used to generate propagating spin waves with wavelengths smaller than the dimensions of the waveguide. This can be overcome by parametric FMR excitation. However, such non-linear effects can be neglected since our simulations are performed using a small oscillating field of 0.1 mT. The extrema of magnetization components during FMR are plotted as a function of PMA in Fig. 3(b). The maximum deviation of magnetization in the y-axis is negligible as seen from the values of $M_{y,min} \sim 1500$ mT in Fig. 3(b). Therefore, the area of the elliptical trajectory on the Bloch's sphere can be assumed to be equal to that of the

projection on the x-z plane. We define the ellipticity $A = m_z/m_x$ and the area of the trajectory as $\pi m_x m_z$, where m_x and m_z are the normalized values of maximum values of M_x and M_z with respect to M_s.

Figure 3(c) shows the change of ellipticity with respect to PMA in the sample $\mu_o H_{ex,y}$ = 100 mT to 150 mT. The ellipticity approaches 1 as the H_p is increases upto the point where the $H_{d,eff} = 0$, while further increase in H_p results in $A > 1$ because $M_z > M_x$. The corresponding areas of precession trajectories are plotted as a function of PMA for different values of $H_{ex,y}$ in Fig. 3(d), which shows that it increases upto $\mu_o H_p \sim 1000$ mT and then gradually decreases for higher values of H_p. Such a behavior can be explained by the fact that while M_z increases monotonically with increasing PMA, M_x increases upto $\mu_o H_p \sim 1000$ mT. Beyond this M_x starts to decrease, until it falls below M_z when $H_p > H_d$ as shown in Fig. 3(b). From this analysis, we see that the ellipticity and the area of precession can be controlled significantly by the PMA. The spin current generated during such a precession is dependent on the magnitudes of the magnetization components which are transverse to the direction of external magnetic field, i.e., M_x and M_z. It was shown that spin pumping efficiency is directly proportional to the area of the elliptical trajectory [10,11]. From our simulations we can see that this area, and hence the pumping efficiency, is strongly dependent on the PMA. The results presented in Fig. 3 show that the pumping efficiency during FMR in an in-plane magnetized CoFeB/MgO junction can be expected to be maximum for $H_p < H_d$, just before the transition of its easy axis from in-plane to perpendicular direction. In terms of spin wave excitation, larger precession cone angles are desirable for improving the spin wave amplitudes [7]. The cone angles which are proportional to the values of M_x and M_z are dependent on the PMA. In CoFeB/MgO junctions, PMA is inversely proportional to the CoFeB thicknesses. Therefore, spin wave amplitudes can be controlled by selecting the CoFeB layer thickness accordingly.

Spin pumping efficiency has been shown to be strongly determined by the ellipticity of a precession trajectory [10,11]. From Fig. 3, it can be seen that the ellipticity $A \sim 0.50$ for the case of 1000 mT < $\mu_o H_p$ < 1130 mT, where the area of precession is found to be maximum. In order to check the validity of this result, simulations were performed at different amplitudes of microwave field. Figure 4(a) shows the magnetization precession trajectories during resonance as a function of the excitation amplitude when $\mu_o H_p = 0$ mT. The ellipticities are found to be independent of the amplitudes of microwave fields as shown in Fig.4(b). The corresponding areas of trajectory as a function of PMA are plotted in Fig. 4(c). It shows that for the range of the applied microwave amplitudes, the area of precession trajectory always has a maximum close to the value of PMA for which $A \sim 0.5$. It should be noted that the error in estimating the area of trajectory on the Bloch's sphere from its projection on the x-z plane is highest around $\mu_o H_p$ = 1000 mT because the oscillation amplitude of M_y is maximum (Fig. 3(b)). Due to this, at higher microwave amplitudes, area is underestimated around $\mu_o H_p$ = 1000 mT and as a result the PMA dependence of area appears to be more flat as microwave amplitudes increase in Fig. 4(c).

IV. Conclusion

In conclusion, we have studied the effect of perpendicular magnetic anisotropy on the magnetization trajectories during ferromagnetic resonance in nanostructured CoFeB using micromagnetic simulations. The two magnetization components transverse to the static field applied in the y-direction was found to have different PMA dependent behavior. While the M_z component increased monotonically with increasing PMA, the M_x component showed a non-monotonous behavior. This results in a non-monotonous PMA dependent area of magnetization trajectory during excitation of FMR. This area is found to be maximum around the condition where M_z:$M_x \sim 1$:2. Such a behavior is found to be independent of the excitation power in the range of applied microwave field amplitudes. Previous studies have shown that area of precession trajectories are proportional to the efficiency of spin pumping [ref]. Further, the spin wave excitation efficiency increases with increasing precession cone angles. Therefore, such an understanding of PMA dependent magnetization trajectories can be used for tuning the intrinsic component of magnetic free energy towards efficient excitation of magnetization dynamics that is required for applications in spin current and spin wave generation.

Acknowledgment

We would like to thank B. Rana for helpful discussions. This work was supported by Grants-in-Aid (18H01862) from JSPS and Materials Science Foundation, Hitachi Metals.

References

[1] J.E. Hirsh, Spin Hall Effect, *Phys. Rev. Lett.*, vol. 83, 1834 (1999).
[2] M. Johnson and R.H. Silsbee, Interfacial charge-spin coupling: Injection and detection of spin magnetization in metals, *Phys. Rev. Lett.*, vol. 55, 1790 (1985).
[3] K. Uchida, S. Takahashi, K. Harii, J. Ieda, W. Koshibae, K. Ando, S. Maekawa and E. Saitoh, Observation of the spin Seebeck effect, *Nature*, vol. 455, pp. 778-781 (2008).
[4] Y. Tserkovnyak, A. Brataas and G.E.W. Bauer, Spin pumping and magnetization dynamics in metallic multilayers, *Phys. Rev. B*, vol. 66, 224403 (2002).
[5] T. Nozaki, Y. Shiota, S. Miwa, S. Murakami, F. Bonell, S. Ishibashi, H. Kubota, K. Yakushiji, T. Saruya, A. Fukushima, S. Yuasa, T. Shinjo and Y. Suzuki, Electric-field-induced ferromagnetic resonance excitation in an ultrathin ferromagnetic metal layer, *Nat. Phys.*, vol. 8, pp. 491–496 (2012).
[6] J. Zhu, J.A. Katine, G. E. Rowlands, Y-J. Chen, Z. Duan, J.G. Alzate, P. Upadhyaya, J. Langer, P.K. Amiri, K.L. Wang and I.N. Krivorotov,

Voltage-Induced Ferromagnetic Resonance in Magnetic Tunnel Junctions, *Phys. Rev. Lett.*, vol. 108, 197203 (2012).

[7] B. Rana, Y. Fukuma, K. Miura, H. Takahashi and Y. Otani, Excitation of coherent propagating spin waves in ultrathin CoFeB film by voltage-controlled magnetic anisotropy, *Appl. Phys. Lett.*, vol. 111, 052404 (2017).

[8] E. Sagasta, Y. Omori, S. Velez, R. Llopis, C. Tollan, A. Chuvillin, L.E. Hueso, M. Gradhand, Y. Otani and F. Casanova, Unveiling the mechanisms of the spin Hall effect in Ta, *Phys. Rev. B*, vol. 98, 060410 (2018).

[9] Y. Fukuma, L. Wang, H. Idzuchi, S. Takahashi, S. Maekawa and Y. Otani, Giant enhancement of spin accumulation and long-distance spin precession in metallic lateral spin valves, *Nat. Mater.*, vol. 10, pp. 527-531 (2011).

[10] K. Ando, T. Yoshino and E. Saitoh, Optimum condition for spin-current generation from magnetization precession in thin film systems, *Appl. Phys. Lett.*, vol. 94, 152509 (2009).

[11] K. Ando, S. Takahashi, J. Ieda, Y. Kajiwara, H. Nakayama, T. Yoshino, K. Harii, Y. Fujikawa, M. Matsuo, S. Maekawa, and E. Saitoh, Inverse spin-Hall effect induced by spin pumping in metallic system, *J. Appl. Phys.*, vol. 109, 103913 (2011).

[12] B. Rana, Y. Fukuma, K. Miura, H. Takahashi and Y. Otani, Effect of excitation power on voltage induced local magnetization dynamics in an ultrathin CoFeB film, *Sci. Rep.*, vol. 7, 2318 (2017).

[13] T. Maruyama, Y. Shiota, T. Nozaki, K. Ohta, N. Toda, M. Mizuguchi, A.A. Tulapurkar, T. Shinjo, M. Shiraishi, Y. Ando and Y. Suzuki, Large voltage-induced magnetic anisotropy change in a few atomic layers of iron, *Nat. Nanotechnol.*, vol. 18, pp. 158-161 (2009).

[14] Y. Shiota, T. Nozaki, F. Bonell, S. Murakami, T. Shinjo and Y. Suzuki, Induction of coherent magnetization switching in a few atomic layers of FeCo using voltage pulses, *Nat. Mater.*, vol. 11, pp. 39–43 (2012).

[15] W. X. Wang, Y. Yang, H. Naganuma, Y. Ando, R. C. Yu, and X. F. Han, The perpendicular anisotropy of Co40Fe40B20 sandwiched between Ta and MgO layers and its application in CoFeB/MgO/CoFeB tunnel junction, *Appl. Phys. Lett.*, vol. 99, 012502 (2011).

[16] S. Ikeda, K. Miura, H. Yamamoto, K. Mizunuma, H.D. Gan, M. Endo, S. Kanai, J. Hayakawa, F. Matsukura and H. Ohno, A perpendicular-anisotropy CoFeB-MgO magnetic tunnel junction, *Nat. Mater.*, vol. 9, pp. 721–724 (2010).

[17] LLG Micromagnetics developed by M.R. Sheinfein and E.A. Price.

[18] J. M. Shaw, H.T. Nembach, M. Weiler, T.J. Silva, M. Schoen, J.Z. Sun and D.C. Worledge, Perpendicular Magnetic Anisotropy and Easy Cone State in Ta/Co60Fe20B20 /MgO, *IEEE Magn. Lett.*, vol. 6, pp. 1-4 (2015).

[19] S. Chikazumi, “International series of monographs on physics 94: Physics of Ferromagnetism”, *Oxford University Press* (2009).

FIGURES

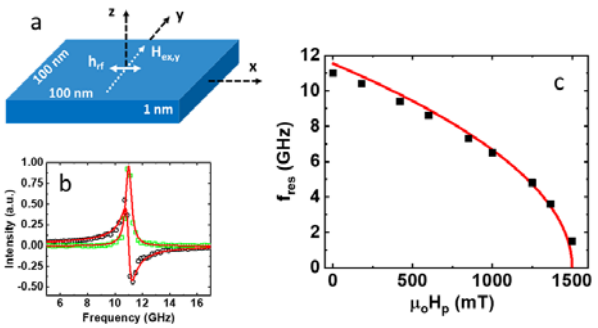

Fig. 1 (a) Schematic of the sample along with dimensions and directions of microwave field h_{rf} and static external field $H_{ex,y}$ used for simulations. A single domain model was assumed throughout and damping constant is taken as $\alpha = 0.02$. FMR simulations are performed in frequency sweep mode. (b) Typical FMR spectra obtained in the frequency sweep mode simulations for $\mu_oH_{ex,y}$ = 100 mT, microwave amplitude $\mu_oh_{rf,x}$ = 0.1 mT and perpendicular magnetic anisotropy field μ_oH_p = 0 mT. Lines are fits using Eq. (1). (c) Resonance frequencies f_{res} as a function of H_p along with fit using Kittel equation.

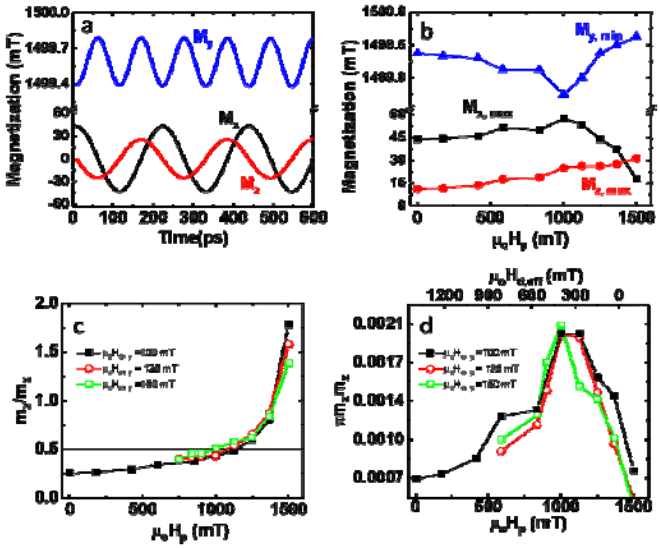

Fig. 3 (a) Magnetization components M_x, M_y and M_z as a function of time during FMR for a sample with μ_oH_p= 1250 mT. (b) Dependence of the maximum values of M_x and M_z and minimum value of M_y as a function of perpendicular magnetic anisotropy. Simulations are performed in a frequency sweep mode at $\mu_oH_{ex,y}$ = 100 mT. (c) Effect of H_p on the ellipticity of the magnetization trajectories during FMR. (d) The corresponding area as a function of H_p. The effective demagnetization field $H_{d,eff}$ corresponding to the PMA field are shown in the top x-axis. Simulations are performed in a frequency sweep mode at $\mu_oH_{ex,y}$ = 100 mT, 125 mT and 150 mT and microwave amplitude $\mu_oh_{rf,x}$ = 0.1 mT.

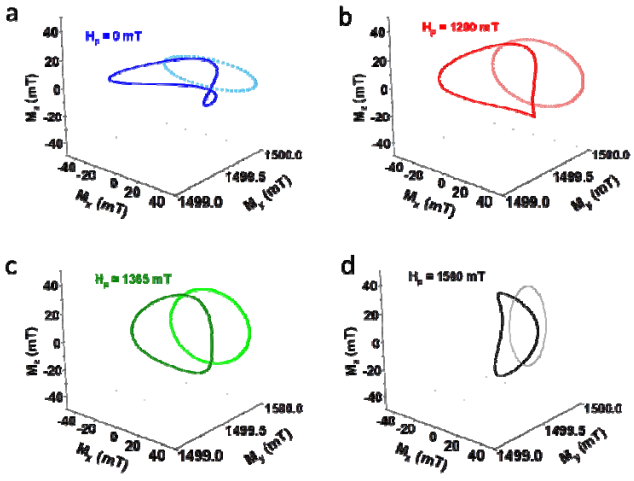

Fig. 2 (a)-(d) Magnetization precession trajectories for μ_oH_p= 0 mT to 1500 mT during FMR. Simulations are performed in a frequency sweep mode at $\mu_oH_{ex,y}$ = 100 mT and microwave amplitude $\mu_oh_{rf,x}$ = 0.1 mT.

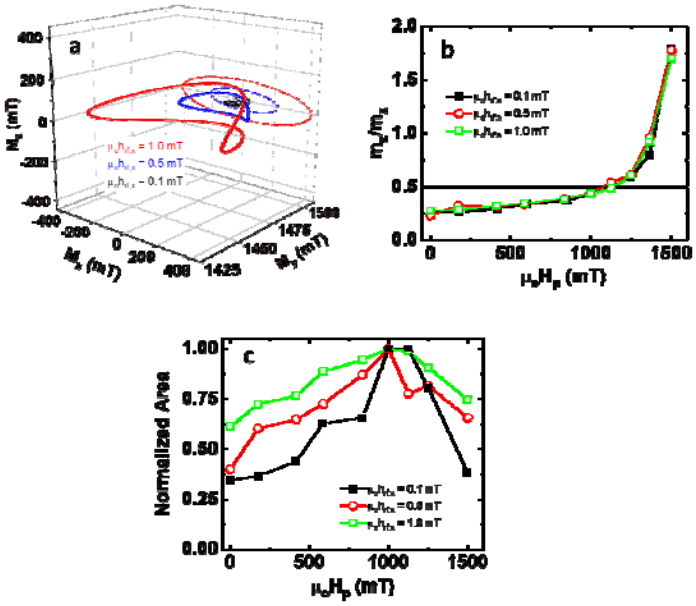

Fig. 4 (a) Magnetization trajectories during FMR at different microwave amplitudes $h_{rf,x}$ at a fixed μ_oH_p= 0 mT and $\mu_oH_{ex,y}$ = 100 mT. (b) Ellipticity and (c) area of magnetization precession trajectories as a function of H_p at different $h_{rf,x}$. The areas are normalized with respect to the maximum value obtained for each $h_{rf,x}$.